Article

Cell Reports

DDX60 Is Involved in RIG-I-Dependent and Independent Antiviral Responses, and Its Function Is Attenuated by Virus-Induced EGFR Activation

Graphical Abstract

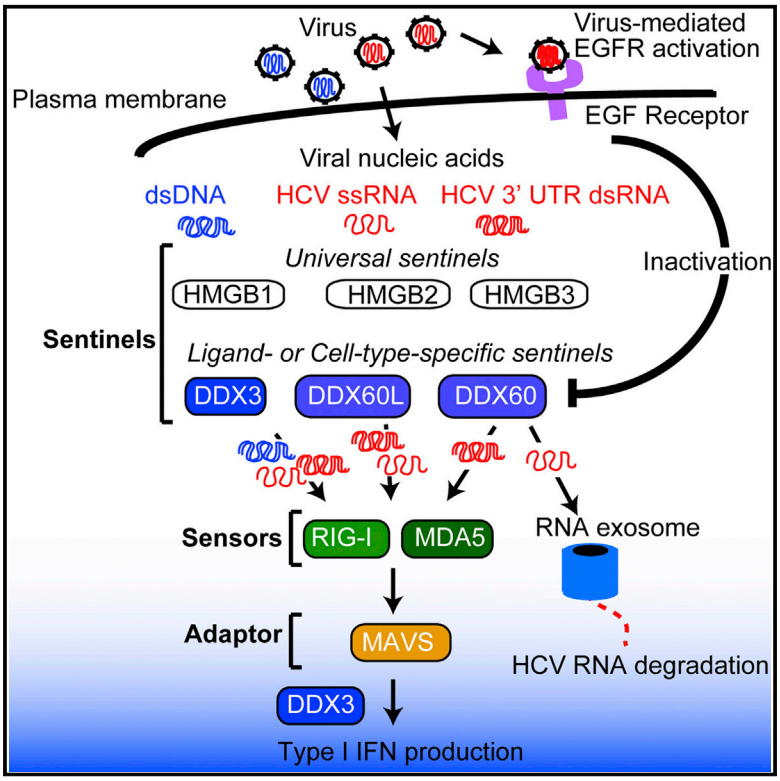

Highlights

- Human DDX60 functions as a ligand-specific sentinel for RIG-I activation
- DDX60 plays a role in RIG-I-mediated innate immune response in vivo
- DDX60 is involved in a viral RNA degradation pathway
- Virus-mediated EGF receptor activation attenuates DDX60 antiviral activities

Authors

Hiroyuki Oshiumi, Moeko Miyashita, ..., Misako Matsumoto, Tsukasa Seya

Correspondence

oshiumi@med.hokudai.ac.jp

In Brief

Type I IFN production and viral RNA degradation are important for antiviral innate immune responses. Oshiumi et al. show that DDX60 is involved in both RIG-I-dependent type I IFN production and RIG-I-independent viral RNA decay pathways and that DDX60 functions as a sentinel for cytoplasmic antiviral innate immune response.

Oshiumi et al., 2015, Cell Reports *11*, 1193–1207
May 26, 2015
http://dx.doi.org/10.1016/j.celrep.2015.04.047

CellPress

Cell Reports
Article

DDX60 Is Involved in RIG-I-Dependent and Independent Antiviral Responses, and Its Function Is Attenuated by Virus-Induced EGFR Activation

Hiroyuki Oshiumi,[1,5,6,*] Moeko Miyashita,[1,4,5] Masaaki Okamoto,[1] Yuka Morioka,[2] Masaru Okabe,[3] Misako Matsumoto,[1] and Tsukasa Seya[1]
[1]Department of Microbiology and Immunology, Graduate School of Medicine, Hokkaido University, Sapporo 060-8638, Japan
[2]Research Center for Infection-Associated Cancer, Division of Disease Model Innovation, Institute of Genetic Medicine, Hokkaido University, Sapporo 060-8638, Japan
[3]Research Institute for Microbial Disease, Osaka University, 3-1 Yamadaoka Suita, Osaka 565-0871, Japan
[4]Hokkaido Pharmaceutical University School of Pharmacy, 7-1 Katsuraoka-cho, Otaru, Hokkaido 047-0246, Japan
[5]Co-first author
[6]Present address: Laboratory for Biologics Development, Research Center for Zoonosis Control, Hokkaido University, Sapporo 060-8638, Japan
*Correspondence: oshiumi@med.hokudai.ac.jp
http://dx.doi.org/10.1016/j.celrep.2015.04.047

SUMMARY

RIG-I-mediated type I interferon (IFN) production and nuclease-mediated viral RNA degradation are essential for antiviral innate immune responses. DDX60 is an IFN-inducible cytoplasmic helicase. Here, we report that DDX60 is a sentinel for both RIG-I activation and viral RNA degradation. We show that DDX60 is an upstream factor of RIG-I that activates RIG-I signaling in a ligand-specific manner. *DDX60* knockout attenuates RIG-I signaling and significantly reduces virus-induced type I IFN production in vivo. In addition, we show that DDX60 is involved in RIG-I-independent viral RNA degradation. DDX60 and RIG-I adaptor MAVS double-knockout mice reveal a role for DDX60-dependent RNA degradation in antiviral responses. Several viruses induced DDX60 phosphorylation via epidermal growth factor receptor (EGFR), leading to attenuation of the DDX60 antiviral activities. Our results define DDX60 as a sentinel for cytoplasmic antiviral response, which is counteracted by virus-mediated EGF receptor activation.

INTRODUCTION

The innate immune system is essential for controlling viral infection. Cytoplasmic viral RNA and polyI:C are recognized by RIG-I-like receptors including RIG-I and MDA5, which trigger the induction of type I and III interferons (IFNs) and other inflammatory cytokines via the MAVS adaptor molecule (also called IPS-1, Cardif, and VISA) (Loo and Gale, 2011). MAVS activates TBK1 protein kinase, leading to autophosphorylation of TBK1 (Soulat et al., 2008). Autophosphorylated TBK1 is essential for IRF-3 phosphorylation, which results in type I IFN expression (Soulat et al., 2008).

The RIG-I protein comprises two N-terminal caspase-activation and recruitment domains (CARDs), a DExD/H box (DDX) helicase domain, and a C-terminal regulatory domain (RD) (Saito et al., 2007). The RD and DDX helicase domains bind double-stranded RNA (dsRNA) (Takahasi et al., 2008), leading to K63-linked polyubiquitination of the RD by the Riplet ubiquitin ligase (Oshiumi et al., 2013). Riplet-mediated ubiquitination allows TRIM25 to access RIG-I CARDs, which is essential for triggering the induction of type I IFN production via the MAVS adaptor (Chan and Gack, 2015; Oshiumi et al., 2013). In contrast, cytoplasmic viral DNA is recognized by DNA sensors, including cyclic GMP-AMP synthase (cGAS), DAI, IFI16, DDX41, and Mre11 (Desmet and Ishii, 2012; Kondo et al., 2013). Chen and colleagues have recently shown that cGAS is essential for type I IFN production in response to viral DNA (Gao et al., 2013; Li et al., 2013a; Sun et al., 2013). Those cytoplasmic nucleic acids sensors require sentinels for recognition of viral RNA and DNA. The high mobility group box proteins, HMGB1, 2, and 3, bind to cytoplasmic immunogenic nucleic acids and function as universal sentinels for RNA and DNA sensors (Yanai et al., 2009).

Approximately 60 genes encode DDX helicases in the human genome. Bowie and colleagues first reported that a member of the DDX superfamily is involved in RIG-I signaling (Schröder et al., 2008; Soulat et al., 2008). Subsequently, other studies have shown that DDX superfamily members such as DDX3, DHX29, DHX36, and DDX60 are involved in RIG-I-dependent type I IFN production in response to viral RNA and DNA (Desmet and Ishii, 2012; Sugimoto et al., 2014; Yoo et al., 2014). However, the in vivo roles of these non-RIG-I-like helicases remain unclear.

DDX60 (also called FLJ20035) is an IFN-inducible gene that has been identified via a microarray analysis of genes induced by viral infection in human dendritic cells (DCs) (Miyashita et al., 2011). The ectopically expressed DDX60 protein associates with RIG-I and promotes RIG-I RNA-binding activity, leading to RIG-I-mediated type I IFN expression (Miyashita et al., 2011). The DDX60 helicase domain binds to viral RNA and DNA, and the DDX60 ATP-binding site is essential for DDX60-mediated

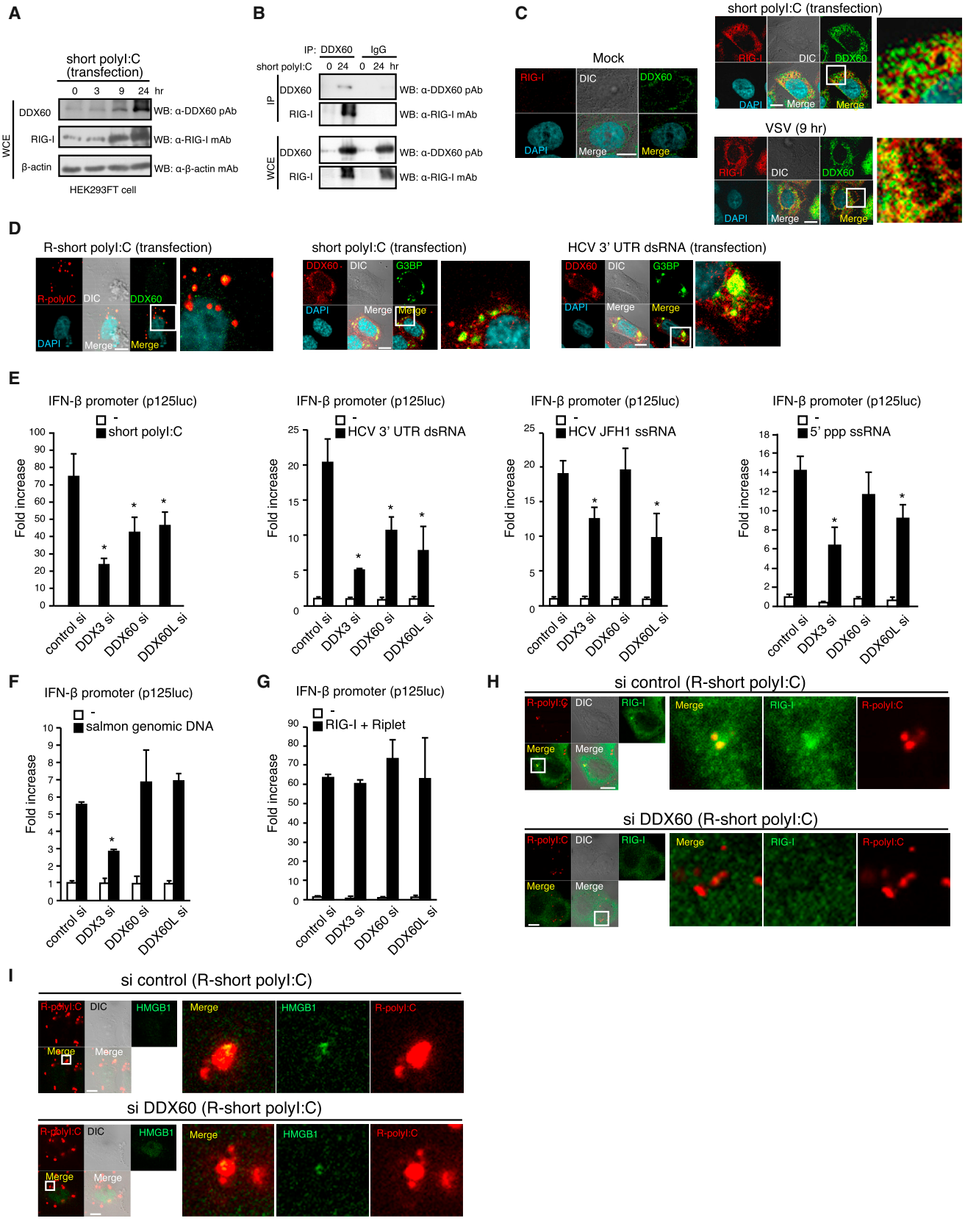

(legend on next page)

RIG-I activation (Miyashita et al., 2011). Genetic studies indicated that DDX60 acts upstream of RIG-I in the innate immune response (Miyashita et al., 2011). In contrast, Rice and colleagues have shown that ectopically expressed DDX60 suppresses hepatitis C virus (HCV) replication in a RIG-I-independent manner (Schoggins et al., 2011); however, the underlying mechanism remains unknown. A *DDX60* paralog, *DDX60L*, is located upstream of *DDX60*, and the DDX60L protein shows similarity to DDX60; however, the function of DDX60L remains unknown.

Cytoplasmic viral RNA degradation pathways are important for the suppression of viral replication. The Xrn1 RNA 5′−3′ exonuclease plays a crucial role in HCV RNA degradation and suppresses HCV replication (Li et al., 2013b). The zinc-finger antiviral protein (ZAP) is a host antiviral factor required for the degradation of viral RNA (Chen et al., 2008; Guo et al., 2007). ZAP associates with components of the RNA exosome, which is a protein complex essential for processing the 3′ end of host and viral RNAs (Houseley et al., 2006). Several DDX helicases are essential for RNA exosome function (Schmid and Jensen, 2008). A phylogenetic analysis indicated that the DDX60 RNA helicase domain is similar to a component of the RNA exosome, Ski2, and DDX60 associates with RNA exosome core components (Miyashita et al., 2011); however, the role of DDX60 in RNA degradation by RNA exosome remains unclear.

HCV, the influenza A virus, and other viruses are known to activate the epidermal growth factor (EGF) receptor, which is a Tyr kinase receptor (Diao et al., 2012; Ueki et al., 2013). Influenza A virus- and respiratory-virus-induced EGF receptor activation suppresses IRF1-induced type III IFN production (Ueki et al., 2013). The HCV-induced EGF receptor activation reduces STAT3 phosphorylation and STAT1 dimerization and attenuates IFN-induced antiviral activities (Lupberger et al., 2013). A previous proteome analysis has shown that DDX60 is phosphorylated by the EGF receptor (Tong et al., 2008); however, the physiological role of DDX60 phosphorylation remains unknown. In this study, we demonstrated that DDX60 plays a crucial role in the antiviral innate immune response in vivo and that the DDX60 antiviral activities are regulated by EGF signaling.

RESULTS

DDX60 Associates with the RIG-I RNA Sensor

First, we investigated the physical interaction between endogenous DDX60 and RIG-I. Endogenous DDX60 protein levels increased after transfection with a RIG-I ligand, short polyI:C (Figure 1A), and endogenous RIG-I was co-immunoprecipitated with endogenous DDX60 protein after short polyI:C transfection (Figure 1B), suggesting a physical interaction between endogenous RIG-I and DDX60. Second, we investigated subcellular localization of DDX60. Endogenous DDX60 protein exhibited a cytoplasmic localization in resting cells, and the DDX60 staining became strong after vesicular stomatitis virus (VSV) infection or transfection with short polyI:C (Figure 1C). Colocalization of DDX60 with RIG-I was detected after VSV infection or stimulation with short polyI:C transfection (Figure 1C). RIG-I localizes at stress granule after stimulation with short polyI:C transfection (Onomoto et al., 2012). As observed for RIG-I, DDX60 colocalized with transfected rhodamine-conjugated short polyI:C (R-polyI:C) and the stress-granule marker G3BP after transfection with short poly I:C or another RIG-I ligand, HCV 3′-UTR dsRNA (Saito et al., 2008) (Figure 1D). Taken together, these data indicate that DDX60 binds to RIG-I after stimulation.

To evaluate the role of DDX60 in RIG-I-mediated signaling, we next investigated the effect of *DDX60* knockdown on RIG-I signaling. *DDX60* knockdown reduced IFN-β promoter activation in response to short polyI:C or HCV 3′ UTR dsRNA transfection (Figure 1E). In contrast, *DDX60* knockdown failed to reduce this promoter activation in response to other RIG-I ligands, in-vitro-transcribed HCV JFH1 single-stranded RNA (ssRNA) (Saito et al., 2008) or a 63-nt 5′ triphosphated ssRNA (5′-ppp ssRNA) (Takahasi et al., 2008) (Figure 1E). Unlike DDX60, knockdown of other DDX superfamily members (DDX60L or DDX30) reduced the promoter activation induced by the four RIG-I ligands (Figures 1E and S1A). *DDX3*, but not *DDX60* or *DDX60L*, knockdown reduced the promoter activation in response to salmon genomic DNA transfection (Figure 1F). These data suggest a ligand-specific involvement of DDX60 in RIG-I signaling.

DDX60, *DDX60L*, and *DDX3* knockdown did not reduce the promoter activation induced by RIG-I and Riplet ectopic expression (Figure 1G). A microscopic analysis showed that RIG-I colocalized with transfected R-polyI:C, whereas colocalization was barely detected in *DDX60*-, *DDX60L*-, and *DDX3*-knockdown cells (Figures 1H and S1B). HMGB1 universal sentinel localization on transfected R-polyI:C was detected even in *DDX60*-, *DDX60L*-, and *DDX3*-knockdown cells (Figures 1I and S1B). Taken together, these data suggest that DDX60 acts upstream of RIG-I.

Figure 1. DDX60 Is a Sentinel Helicase for Cytoplasmic Viral RNA Sensor RIG-I

(A and B) HEK293FT cells were stimulated with short polyI:C transfection. Whole-cell extract (WCE) was prepared at the indicated time points. Immunoprecipitation (IP) was performed with antibody to DDX60 or control immunoglobulin G (IgG). The samples were analyzed by immunoblot assay using anti-RIG-I, anti-DDX60, and anti-β-actin antibodies.

(C and D) HeLa cells were infected with VSV for 9 hr or transfected with short polyI:C, rhodamine-conjugated short polyI:C (R-polyI:C), or HCV 3′-UTR dsRNA for 6 hr, then fixed and stained for RIG-I, DDX60, or G3BP and with DAPI.

(E and F) siRNAs for negative control, *DDX3*, *DDX60*, and *DDX60L* were transfected into HEK293 cells for 48–72 hr. Short polyI:C, HCV 3′ UTR dsRNA, HCVJFH1 ssRNA, 63 bp of 5′-triphosphated ssRNA (5′-ppp ssRNA), or salmon sperm genomic DNA was transfected into HEK293 cells with p125luc and *Renilla* luciferase (internal control) vectors for 24 hr, and luciferase activity was determined.

(G) siRNAs as indicated were transfected into HEK293 cells for 48 hr. RIG-I and Riplet expression vectors were transfected into HEK293 cells together with p125luc and *Renilla* luciferase vectors for 24 hr, and luciferase activity was determined.

(H and I) siRNAs as indicted were transfected into HeLa cells for 48 hr. R-polyI:C was transfected into HeLa cells for 6 hr (H) or 16 hr (I), and the cells were fixed and stained with anti-RIG-I (H) or anti-HMGB1 (I) antibody. The localizations of R-polyI:C and the endogenous proteins were observed with confocal microscopy. The scale bar represents 10 μm. Data are presented as mean ± SD. See also Figure S1.

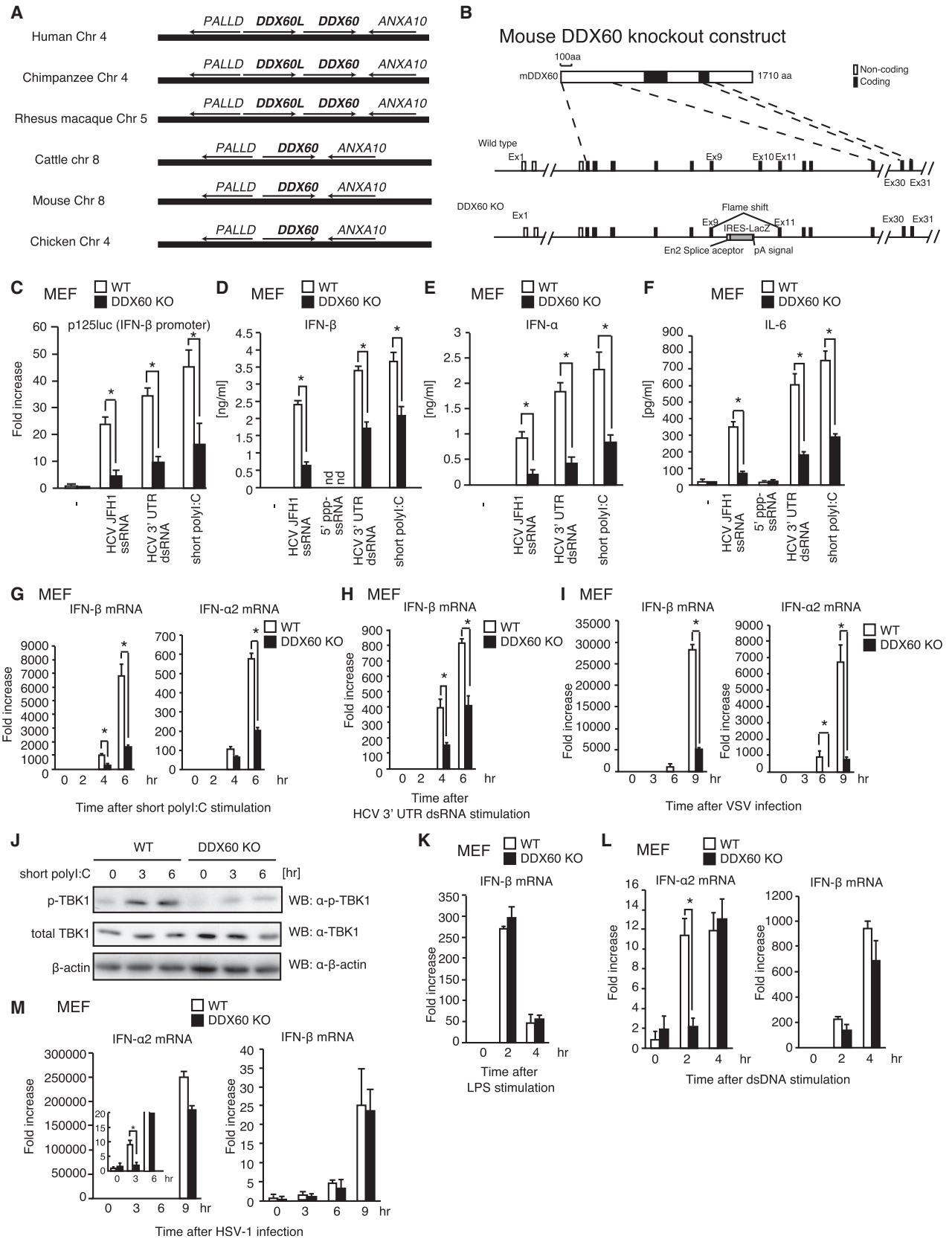

(legend on next page)

Generation of *DDX60*-Deficient Mice

Human *DDX60* and *DDX60L* are located in tandem on chromosome IV (Figure 2A). *DDX60L* mRNA was expressed in lymph node, prostate, stomach, thyroid, tongue, and trachea and was induced by type I IFN stimulation in HeLa cells as *DDX60* (Figures S2A and S2B). The phylogenetic tree constructed with DDX60 and DDX60L protein sequences indicated that mouse *DDX60* is an ortholog of human *DDX60*, but not *DDX60L* (Figure S2C).

To further clarify the role of DDX60 in the RIG-I-dependent pathway, we generated a *DDX60*-deficient mouse. Exon 10 of mouse *DDX60* was removed by a gene-targeting method (Figure 2B). RNA expression of exon 10 was not detected in the *DDX60*-homozygous mutants, and expression of exon 30–31 regions was lower than 5% of the expression level detected in wild-type (WT) mice (Figure S2D). RIG-I, MDA5, MAVS, TICAM-1, and TLR3 expression was not affected by the *DDX60* mutation (Figure S2E). *DDX60*-knockout (*DDX60*-KO) mice were born at the expected Mendelian ratio and exhibited normal development and breading (Figure S2F).

Mouse DDX60 Is Involved in the RIG-I-Dependent Type I IFN Expression Pathway

WT and *DDX60*-KO mouse embryonic fibroblast (MEF) cells were stimulated with HCV JFH1 ssRNA, HCV 3′ UTR dsRNA, or short polyI:C transfection, and the activation of the IFN-β promoter was determined by reporter-gene assay. Unlike human DDX60, mouse DDX60 was required for promoter activation in response to all three RIG-I ligands (Figure 2C). We determined the IFN-α, IFN-β, and interleukin-6 (IL-6) protein levels in culture medium by ELISA. *DDX60* KO reduced IFN-α, IFN-β, and IL-6 production from MEFs in response to the three RIG-I ligands (Figures 2D–2F), whereas residual type I IFN and IL-6 production was still detected in *DDX60* KO MEFs (Figures 2D–2F). These data indicate the existence of DDX60-dependent and DDX60-independent pathways during RIG-I activation. Unlike HEK293 cells, 5′-ppp ssRNA did not induce IFN-β and IL-6 production from MEFs (Figures 2D and 2F).

DDX60 KO reduced the endogenous IFN-β and IFN-α2 mRNA expression induced by short polyI:C, HCV 3′ UTR dsRNA, or VSV infection (Figures 2G–2I). VSV-induced IFN-λ2/3 mRNA expression was also reduced by *DDX60* KO (see below). TBK1 phosphorylation was induced by short polyI:C transfection, and *DDX60* KO reduced the phosphorylation of TBK1 (Figure 2J). In contrast, IFN-β and IFN-α2 mRNA expression induced by lipopolysaccharide (LPS) stimulation were comparable between WT and *DDX60* KO MEFs (Figure 2K). *DDX60* KO reduced dsDNA- or HSV-1-induced IFN-α2 mRNA expression only at early time points and failed to reduce IFN-β mRNA expression (Figures 2L and 2M). Taken together, our data demonstrate that DDX60 plays a crucial role for RIG-I activation in fibroblast cells.

Although DDX60 was ubiquitously expressed in mouse tissues, its expression level was different among different tissues (Figure 3A). Bone-marrow-derived dendritic cells (BM-DCs) robustly expressed DDX3 and DHX36, which are involved in the RIG-I activation pathway (Oshiumi et al., 2010b; Yoo et al., 2014), whereas DDX60 was exclusively expressed in peritoneal macrophages (Figure 3A).

Next, we examined the role of DDX60 in DCs and macrophages. Interestingly, *DDX60* KO reduced virus- or RIG-I-ligand-induced IFN-α and IFN-β production in peritoneal macrophages, but not in BM-DCs (Figure 3B–3E). Next, we investigated the role of DDX60 in splenic CD11c$^+$ cells. KO of *DDX60* also reduced type I IFN production from splenic CD11c$^+$ cells after VSV infection (Figure S3). These data indicated that DDX60 is required for RIG-I-mediated type I IFN production in peritoneal macrophages and splenic CD11c$^+$ cells, and our data also indicate a cell-type-specific role of DDX60 in RIG-I activation.

DDX60 KO reduced HSV-1-induced IFN-α production in peritoneal macrophages (Figure 3F), whereas DDX60 was dispensable for HSV-1-induced IFN-β production in BM-DCs or peritoneal macrophages (Figure 3F and 3G). These data suggest that DDX60 plays only a minor role in the DNA-sensing pathway.

DDX60 Plays a Crucial Role in Type I IFN Production In Vivo

Next, we investigated the in vivo role of DDX60. First, we observed type I IFN levels in sera after intraperitoneal injection of short polyI:C. Serum IFN-β levels in *DDX60*-KO mice were comparable to those of WT mice (Figure 4A).

Second, we observed hepatic type I IFN expression in response to hydrodynamically injected HCV RNA as described previously (Okamoto et al., 2014; Saito et al., 2008). *RIG-I* KO abolishes hepatic type I IFN expression in response to hydrodynamically injected HCV JFH1 ssRNA (Saito et al., 2008). Although HCV RNA levels in *DDX60*-KO mouse livers were slightly higher than those detected in WT mouse livers (Figure 4B), *DDX60* KO markedly reduced hepatic IFN-β and IFN-α2 mRNA levels and serum IFN-β protein levels after hydrodynamic injection (Figures 4C and 4D).

Third, we investigated in vivo the antiviral innate immune response after intraperitoneal VSV infection. *DDX60* KO reduced

Figure 2. DDX60 Plays a Crucial Role in Type I IFN Expression in MEFs

(A) Schematic representation of *PALLD-ANXA10* loci of human, chimpanzee, *Rhesus macaque*, cattle, mouse, and chicken.

(B) Schematic representation of *DDX60* locus showing its exon (boxes) and introns (lines). Exon 10 was replaced with the gene cassette.

(C) Wild-type (WT) and *DDX60* KO MEFs were transfected with 0.1 μg HCV JFH1 ssRNA, HCV 3′ UTR dsRNA, or short polyI:C for 24 hr together with p125luc and *Renilla* luciferase vectors, and luciferase activity was subsequently determined.

(D–I) WT and *DDX60* KO MEFs were transfected with indicated ligand or infected with VSV (MOI = 10). 24 hr after stimulation, type I IFN (D and E) and IL-6 (F) protein levels in culture medium were determined by ELISA. Type I IFN mRNA expression at indicated time point was determined by qRT-PCR (G–I).

(J) WT and *DDX60* KO MEFs were stimulated with short polyI:C transfection. Whole-cell lysate was prepared at the indicated time points and subjected to SDS-PAGE and immunoblot analysis using anti-phospho-TBK1 (p-TBK1), TBK1 (total TBK1), and β-actin antibodies.

(K–M) WT and *DDX60* KO MEFs were stimulated with LPS (K) or salmon genomic DNA (dsDNA) transfection (L) or infected with HSV-1 (M). RNA was extracted at indicated time points, and IFN-α2 and IFN-β mRNA expressions were determined by qRT-PCR.

Data are presented as mean ± SD. See also Figure S2.

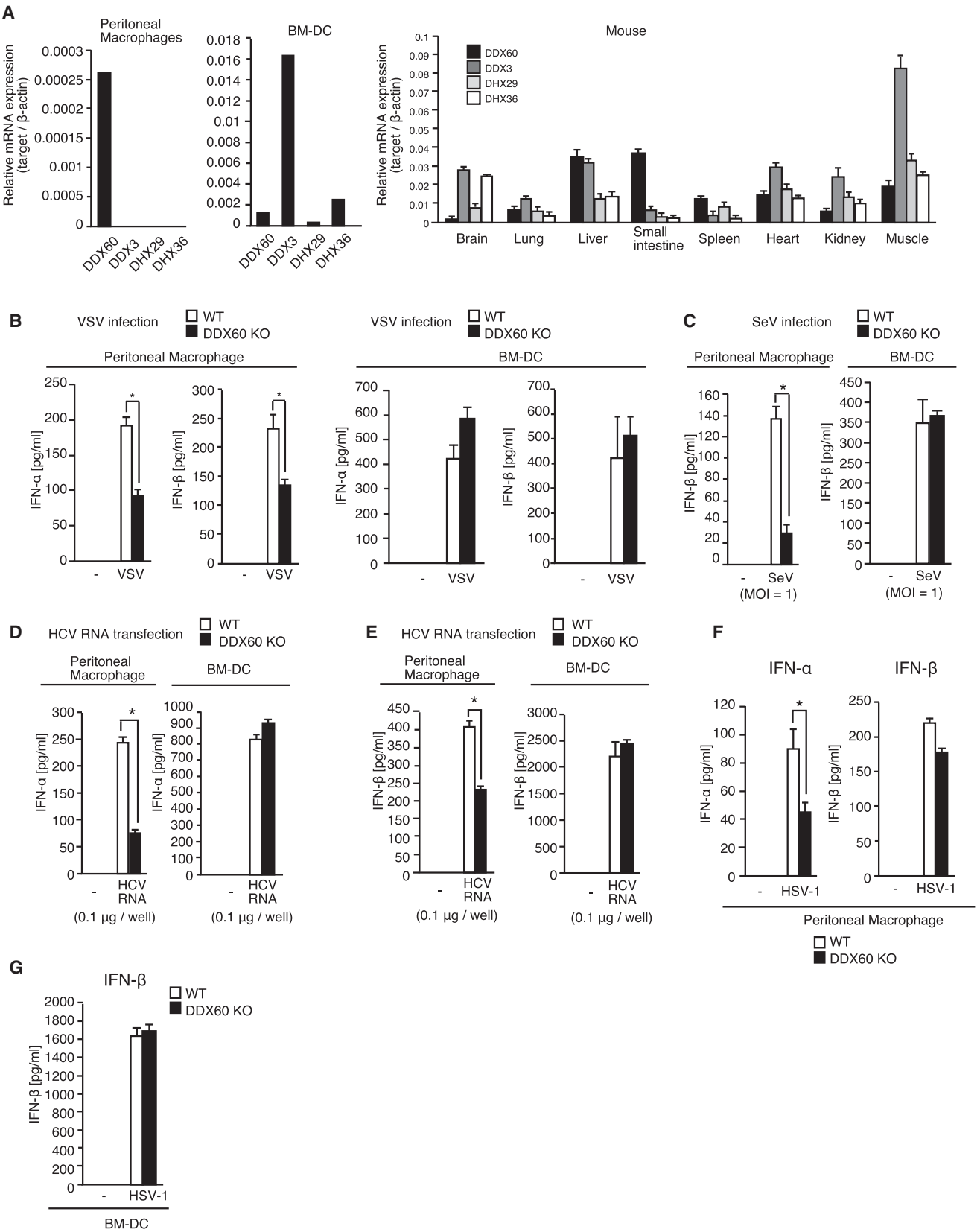

(legend on next page)

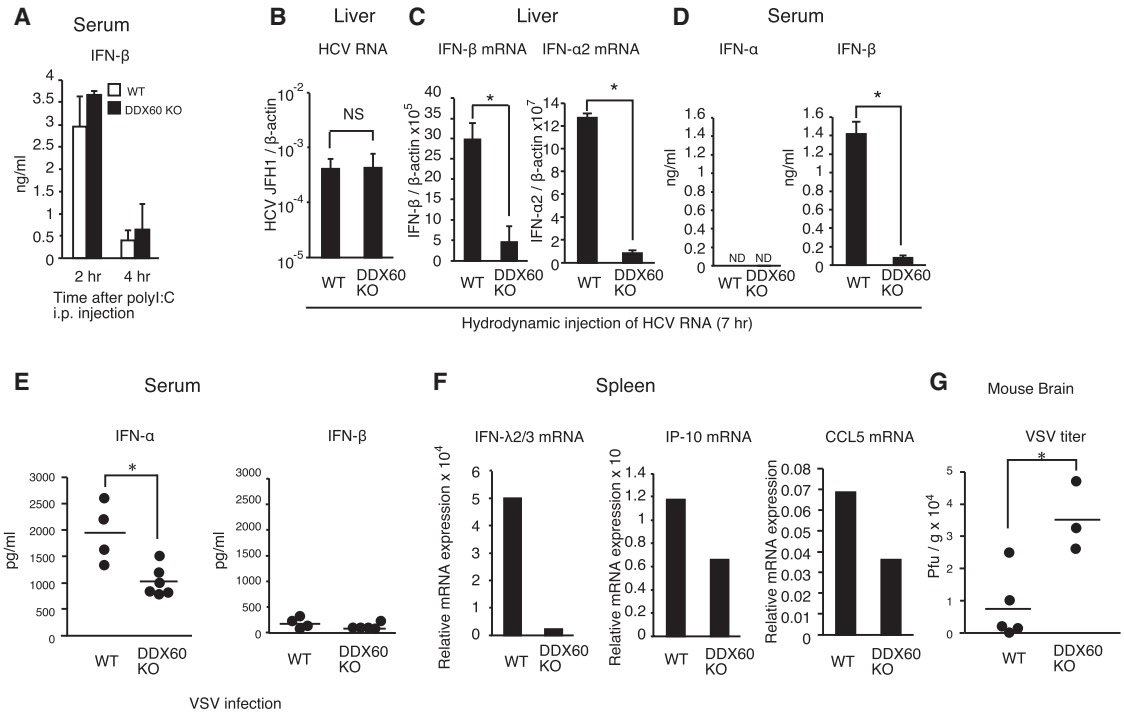

Figure 4. DDX60 Plays a Crucial Role in Antiviral Innate Immune Responses In Vivo

(A) 50 μg poly I:C was intraperitoneally (i.p.) injected into WT and *DDX60*-deficient mice. Serum IFN-β levels were determined by ELISA (mean ± SD; n = 3).

(B–D) In vitro synthesized HCV JHF-1 GND ssRNA was hydrodynamically injected into wild-type (WT) and *DDX60* KO mice. 7 hr after hydrodynamic injection, total RNA was extracted from mouse livers, and HCV RNA levels (B) and IFN-α2 and IFN-β mRNA expression levels (C) were determined by qRT-PCR and normalized to β-actin levels. The IFN-α and IFN-β protein levels in sera 7 hr after hydrodynamic injection were determined by ELISA (D). Data are presented as mean ± SD.

(E and F) 1 × 10^7 plaque-forming units (PFU) of VSV was i.p. injected into WT and *DDX60*-deficient mice. 14 hr after infection, IFN-α and IFN-β levels in sera were determined by ELISA (E). Splenic IP-10, CCL5, and IFN-λ2/3 mRNA expression was determined by qRT-PCR and normalized to β-actin (F).

(G) WT and *DDX60* KO mice were intranasally infected with 2 × 10^6 PFU of VSV and sacrificed on day 4 after infection. Titers in mouse brain were determined by the plaque assay.

See also Figure S4.

serum IFN-α protein levels after VSV infection, and VSV-induced splenic IP-10, CCL5, and IFN-λ2/3 mRNA expression was also reduced by *DDX60* KO (Figures 4E and 4F). *DDX60* KO significantly increased viral titers in mouse brain after intranasal VSV infection (Figure 4G). VSV RNA levels in mouse brain and lung were also increased by *DDX60* KO (Figure S4). These data indicate that DDX60 plays a crucial role in the RIG-I-dependent innate immune response in vivo.

EGF Attenuates RIG-I Signaling via DDX60 Phosphorylation

Next, we focused on regulatory mechanism of DDX60 function. Several viruses activate the EGF receptor to facilitate viral infection (Ueki et al., 2013). A recent mass-spectrometry analysis has shown that two tyrosine residues of DDX60 (Tyr-793 and Tyr-796) are phosphorylated by the EGF receptor (Tong et al., 2008). The two residues are located in the vicinity of the Lys-791 residue, which is important for DDX60 ATP-binding activity (Figure 5A); moreover, the K791A mutation is known to reduce DDX60-dependent RIG-I activation (Miyashita et al., 2011). Thus, we investigated whether EGF receptor activation attenuates the antiviral innate immune response via DDX60 phosphorylation.

First, we examined whether the activation of the EGF receptor induces DDX60 Tyr phosphorylation. For this purpose, we constructed a DDX60-YF mutant, in which Tyr-793 and Tyr-796

Figure 3. Cell-Type-Specific Role of DDX60 in Type I IFN Expression

(A) Total RNA was extracted from BM-DCs, peritoneal macrophages, and mouse tissues as indicated. The mRNA of each DDX gene was determined by qRT-PCR and normalized to β-actin.

(B–G) Wild-type (WT) and *DDX60*-KO peritoneal macrophages and BM-DCs were infected with VSV (B), SeV (C), or HSV-1 (F and G) for 16 hr or transfected with 0.1 μg HCV 3′ UTR dsRNA (HCV RNA) for 16 hr (D and E), and then IFN-α and IFN-β levels in culture medium were determined by ELISA. The results are expressed as means ± SD (n = 3).

See also Figure S3.

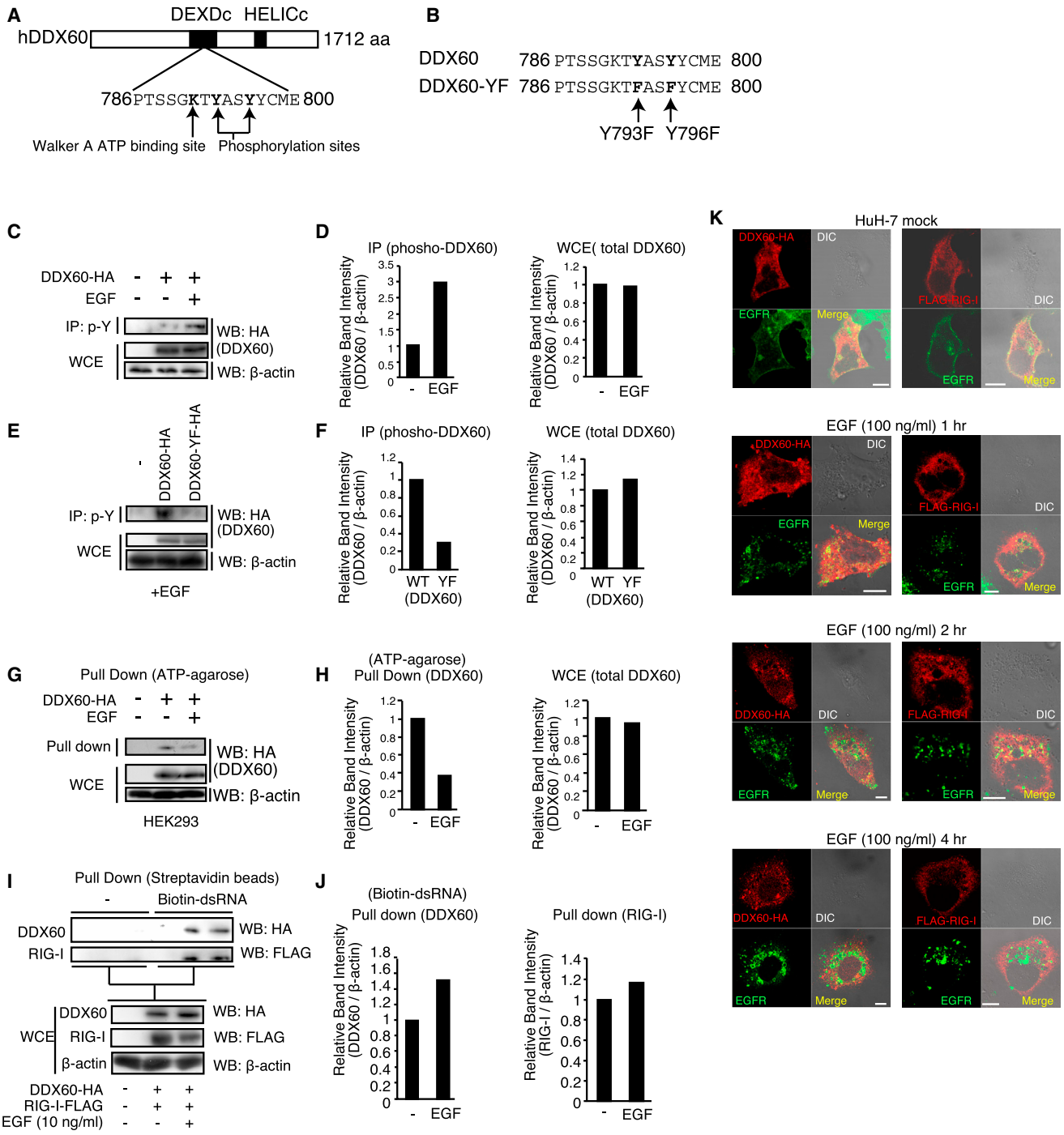

Figure 5. EGF-Induced DDX60 Phosphorylation Impairs DDX60 ATP-Binding Activity

(A and B) Schematic representation of the DDX60 ATP-binding site (A) and a DDX60-YF mutant (B).

(C and D) HEK293 cells were cultured in medium supplemented with or without 10 ng/ml EGF and transfected with a vector carrying HA-tagged DDX60 for 24 hr. Lysates were immunoprecipitated with anti-phospho-tyrosine (p-Y) antibody. The proteins were detected with anti-HA and β-actin antibodies (C). The band intensities were normalized to β-actin intensity (D).

(E and F) HEK293 cells were cultured in medium supplemented with 10 ng/ml EGF and transfected with a vector carrying HA-tagged DDX60 or DDX60-YF for 24 hr. Lysates were immunoprecipitated with anti-p-Y antibody. The proteins were detected with anti-HA and β-actin antibodies (E). The band intensities were normalized to β-actin intensity (F).

(legend continued on next page)

were replaced with Phe residues (Figure 5B). HEK293 cells expressing hemagglutinin (HA)-tagged DDX60 were cultured in medium supplemented with or without 10 ng/ml EGF for 24 hr. A cell lysate was prepared, and phospho-Tyr (p-Y) proteins were subsequently immunoprecipitated using an anti-p-Y antibody. The precipitated phospho-DDX60 (p-DDX60) proteins were detected by western blotting. We found that p-DDX60 was significantly increased by EGF treatment (Figure 5C and 5D) and that the DDX60-YF mutation reduced EGF-induced DDX60 Tyr-phosphorylation (Figures 5E and 5F). This indicated that the phosphorylation of DDX60 Tyr-793 and Tyr-796 was induced by EGF treatment.

Second, we investigated the effect of Tyr phosphorylation on DDX60 function. To test the ATP-binding activity, we performed a pull-down assay with ATP-analog-conjugated agarose beads. Interestingly, EGF treatment reduced DDX60-ATP binding activity (Figures 5G and 5H). Next, we investigated the RNA-binding activity of DDX60 by a pull-down assay with biotin-conjugated dsRNA. EGF treatment did not reduce DDX60 RNA-binding activity (Figures 5I and 5J). Microscopic observation showed that ectopically expressed DDX60 was partially colocalized with the EGF receptor before and after EGF treatment, and DDX60 aggregates appeared after EGF treatment (Figures 5K and S5).

Third, we investigated whether endogenous DDX60 Tyr phosphorylation is induced by the EGF treatment. To test this possibility, we used a proximity ligation assay (PLA), which enables the visualization of endogenous protein modification (Jarvius et al., 2007). We used anti-DDX60 and anti-p-Y antibodies. If endogenous DDX60 Tyr residues are phosphorylated after EGF treatment, it is expected that the PLA-positive (p-Y-DDX60) signals will increase. As expected, the p-Y-DDX60 signals were increased by EGF treatment in HeLa and HuH-7 cells (Figures 6A–6D).

Fourth, we investigated the effect of EGF on endogenous DDX60 function. If EGF treatment impairs DDX60-dependent RIG-I activation, it will reduce RIG-I signaling. As expected, EGF treatment reduced IFN-β and IFN-λ1 promoter activation induced by short polyI:C transfection in HEK293, HuH-7, and MEF cells (Figures 6E and 6F). Long polyI:C-mediated IFN-β promoter activation was moderately reduced by EGF treatment (Figure 6G). Conversely, knockdown of the EGF receptor enhanced short polyI:C-induced IFN-β promoter activation (Figure 6H). VSV-induced IRF3 phosphorylation and IFN-β expression was also enhanced by EGF receptor knockdown (Figures 6I and 6J). In contrast, MAVS-induced IFN-β promoter activation was not reduced by EGF treatment (Figure 6K). Overexpression of DDX60-YF, which is resistant to EGF, canceled the EGF effect on IFN-β promoter activation (Figure 6L), suggesting that EGF treatment reduces IFN-β promoter activation via DDX60. Moreover, EGF treatment reduced polyI:C-induced IFN-β promoter activation in WT MEFs, but not in *DDX60*-KO MEFs (Figure 6M). Taken together, these data indicate that EGF treatment attenuates RIG-I-mediated IFN-β promoter activation via DDX60 phosphorylation.

Viruses Modulate DDX60 Function via EGF Signaling

Influenza A virus and HCV activate the EGF receptor, and inhibitors of the EGF receptor augment innate immune responses during viral infections (Lupberger et al., 2013; Ueki et al., 2013). We performed a PLA and found that influenza A virus infection increased p-Y-DDX60 signals and HCV infection induced p-Y-DDX60 signals (Figures 6N, 6O, and S6A), suggesting that influenza A virus and HCV induce endogenous DDX60 phosphorylation. We found that colocalization of endogenous DDX60 and EGF receptor increased after influenza A virus infection (Figures 6P and 6Q). EGF treatment reduced VSV- or influenza A virus-induced IFN-β, IP10, and tumor necrosis factor α (TNF-α) mRNA expression in HeLa cells, which were cultured in serum-free medium (Figures S6B and S6C), and an EGF receptor inhibitor, erlotinib, increased influenza A virus-induced IFN-β and IP10 mRNA expression (Figure S6D). To investigate the role of DDX60 in the EGF-mediated suppression during viral infection, WT and *DDX60* KO MEFs were infected with VSV in the presence or absence of EGF. Although *DDX60* KO reduced VSV-induced IFN-β and IFN-λ2/3 expression in MEFs cultured in serum-free medium, *DDX60* KO failed to reduce IFN expression in cells cultured in serum-free medium supplemented with 10 ng/ml EGF (Figure 6R). Taken together, these data indicate that virus induces DDX60 phosphorylation via EGF receptor activation, which results in attenuation of DDX60-dependent RIG-I activation.

DDX60 Is Involved in a Viral RNA Degradation Pathway

Previously, Rice and colleagues have reported that ectopically expressed DDX60 suppresses HCV replication in a RIG-I-independent manner (Schoggins et al., 2011). Although Riplet and MAVS were inactivated in a hepatocyte cell line (O cells) that contained HCV 1b full-length replicons (Oshiumi et al., 2013), *DDX60* knockdown increased HCV RNA levels in O cells (Figure 7A), suggesting the existence of RIG-I-independent DDX60 antiviral activity. Thus, we next investigated the RIG-I-independent antiviral activity. DDX60 is similar to SKI2, a component of the RNA exosome, which degrades host and viral RNAs. Small interfering RNA (siRNA) for EXOSC4, a core component of the RNA exosome, also increased HCV RNA levels in O cells

(G and H) HEK293 cells were cultured in medium supplemented with or without 10 ng/ml EGF for 24 hr, and then HA-tagged DDX60 was transfected. 24 hr after transfection, cell lysates were prepared, and then a pull-down assay was performed with ATP analog-agarose. Bound proteins were analyzed by immunoblotting with anti-HA and β-actin antibodies (G). The band intensities were normalized to β-actin intensity (H).
(I and J) HEK293 cells were cultured in medium supplemented with or without 10 ng/ml EGF for 24 hr, and HA-tagged DDX60 and/or FLAG-tagged RIG-I expression vectors were transfected. 24 hr after transfection, a pull-down assay was performed with biotin-conjugated dsRNA. Bound proteins were analyzed by immunoblotting with anti-HA and FLAG antibodies (I). The band intensities were normalized to β-actin intensity (J).
(K) HuH-7 cells were transfected with DDX60-HA or FLAG-RIG-I expressing vector for 24 hr, then stimulated with mock or 100 ng/ml EGF. Cells were fixed at indicated time points and stained with anti-EGFR and anti-HA or -FLAG antibodies. The scale bar represents 10 μm.
See also Figure S5.

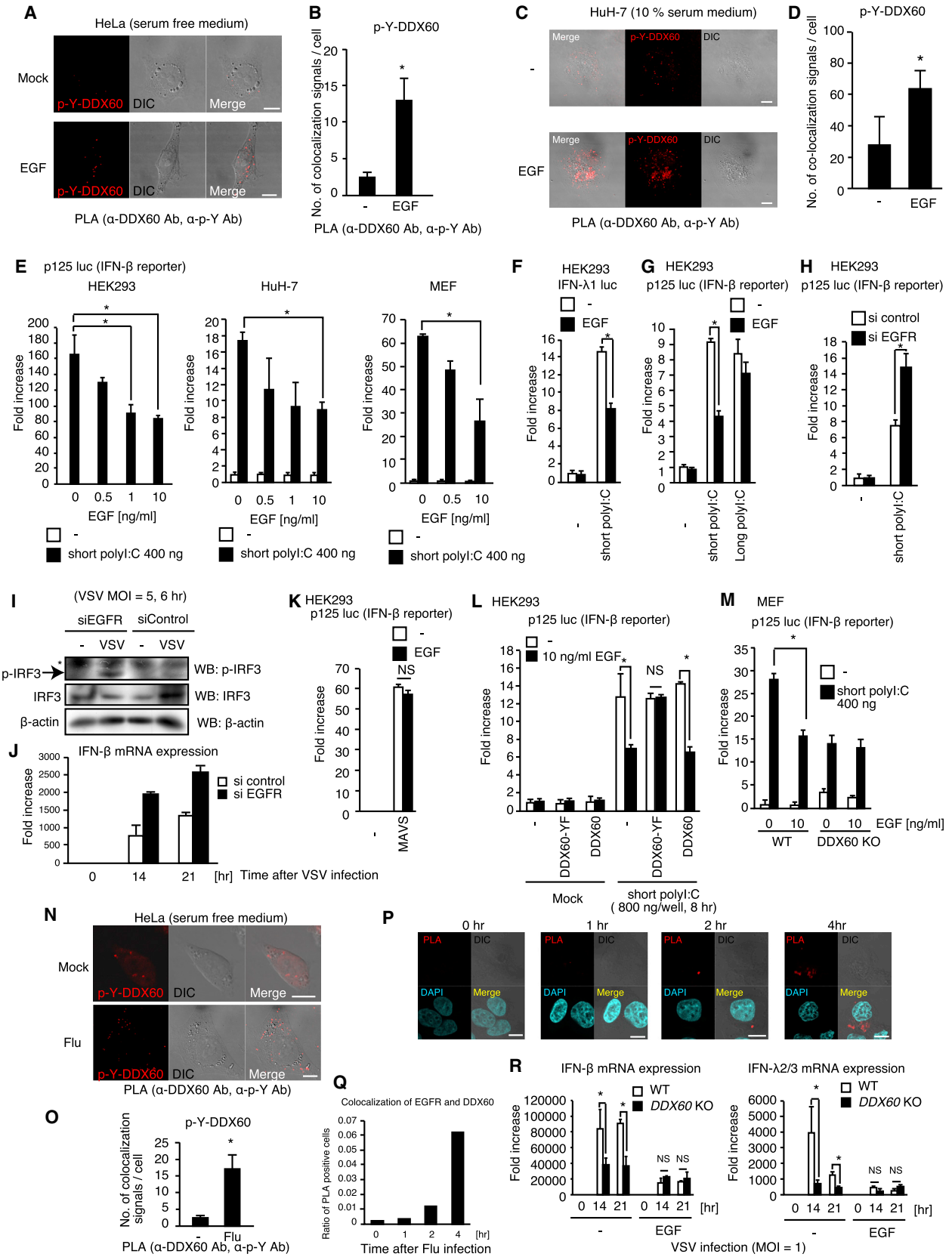

(legend on next page)

(Figure 7B). To test the role of DDX60 in viral RNA degradation, we carried out electroporation assay as described before (Li et al., 2013b). A replication defective HCV JFH1-GND ssRNA was electroporated into HuH-7.5 cells, and viral RNA levels were subsequently determined by qRT-PCR. As expected, *DDX60* knockdown delayed HCV RNA degradation in HuH-7.5 cells or RIG-I knockdown HuH-7 cells (Figures 7C and 7D). Next, we used an inhibitor for HCV polymerase, MK-0608, and investigated viral RNA decay as described previously (Sedano and Sarnow, 2014). siRNA for *DDX60* delayed the HCV RNA decay after addition of the inhibitor (Figure 6E). As seen with *DDX60* knockdown, *EXOSC4* knockdown also delayed the degradation of electroporated HCV RNA in HuH-7.5 cells (Figure 7F), and co-localization of endogenous DDX60 with EXOSC4 was detected in O cells (Figure 7G). These data indicate that DDX60 is involved in HCV RNA degradation. To further corroborate the RIG-I-independent DDX60 function, we investigated the DDX60 antiviral activity in RIG-I-deficient HuH7.5 cells (Saito et al., 2007). We found that siRNA for *DDX60* augmented cytopathic effect of VSV on HuH-7.5 cells and increased VSV titer in culture medium (Figure 7H), and siRNA for *DDX60* delayed VSV dsRNA degradation (Figure 7I). The degradation of VSV dsRNA or HCV JFH1 GND ssRNA was also delayed in *DDX60* KO MEFs (Figures 7J and 7K). Collectively, our data indicate that DDX60 is involved in a RIG-I-independent viral RNA degradation pathway. We also observed that erlotinib treatment increased HCV RNA degradation and reduced HCV RNA levels in O cells (Figures 7L and 7M), indicating that EGF receptor activation attenuates not only DDX60-dependent RIG-I signaling but also DDX60-dependent viral RNA degradation.

To investigate the role of DDX60 in antiviral response in vivo, WT and *DDX60*-KO mice were intranasally infected with VSV, and survival was monitored. *DDX60* KO increased mortality after viral infection (Figure 7N). Next, we assessed the in vivo role of RIG-I-independent DDX60 antiviral activity. We compared the survival of *MAVS* and *DDX60* double-KO mice with *MAVS* single-KO mice after VSV infection. Interestingly, the double-KO mice were more susceptible to VSV than *MAVS* single-KO mice (Figure 7O), suggesting that RIG-I-independent DDX60 antiviral activity plays a crucial role in in vivo antiviral response.

DISCUSSION

DDX60 is an IFN-inducible gene, and the ectopically expressed DDX60 protein associates with RIG-I (Miyashita et al., 2011). Here, we demonstrated that DDX60 co-localized with the RIG-I protein, RIG-I ligand, and a stress granule marker, G3BP, where RIG-I recognizes viral RNA (Onomoto et al., 2012). We also showed that DDX60 bound to RIG-I after stimulation. Considering that DDX60 acts upstream of RIG-I, our data support a model in which DDX60 functions as a sentinel for RIG-I activation. Cytoplasmic HMGBs bind to all immunogenic nucleic acids and function as universal sentinels for RIG-I activation (Yanai et al., 2009). In contrast, our data indicate the ligand-specific involvement of DDX60 in RIG-I activation. These observations suggest that RIG-I requires not only universal sentinels but also ligand-specific sentinels for its activation. It is notable that other DDX helicases, such as DDX3 and DDX60L, exhibited different specificities to nucleic acids. Helicase-related Snf2 family enzymes are known to translocate DNA-associated proteins to regulate nucleic acid metabolism, such as transcription or homologous recombination (Kingston and Narlikar, 1999; Solinger et al., 2002). Considering that DDX3 and DDX60 increase RIG-I binding to dsRNA (Miyashita et al., 2011; Oshiumi et al., 2010b), these DDX helicases might be required to translocate RNA-associated proteins to promote RIG-I recognition of viral RNA.

Figure 6. EGF Induces Endogenous DDX60 Phosphorylation and Suppresses Type I IFN Expression

(A–D) HeLa cells cultured in serum-free medium (A and B) and HuH-7 cells in 10% serum medium (C and D) were stimulated with or without 100 ng/ml EGF for 16 hr, then fixed and stained with anti-DDX60 and anti-p-Y antibodies. Co-localization of DDX60 and p-Y (p-Y-DDX60) was detected by PLA (A and C). The number of co-localization signals (PLA signals: p-Y-DDX60) per cell was counted (means ± SD; n > 10) (B and D).

(E) HEK293, HuH-7, and immortalized MEF cells were cultured in medium supplemented with 0, 0.5, 1, or 10 ng/ml EGF and then transfected with an IFN-β reporter (p125 luc) and *Renilla* luciferase together with or without short polyI:C. 24 hr after transfection, luciferase activity was determined. The results expressed as means ± SD (n = 3).

(F and G) HEK293 cells cultured in medium supplemented with 0 or 10 ng/ml EGF were transfected with IFN-λ1 (F) or IFN-β reporter (p125 luc) (G) plasmid together with *Renilla* luciferase vector. 24 hr after transfection, cells were stimulated with short or long polyI:C transfection for 8 hr, and luciferase activity was determined.

(H–J) HEK293 cells cultured with or without 500 pg/ml EGF were transfected with siRNA for negative control or EGF receptor. The luciferase activities induced by short polyI:C was determined as in (G), and IRF3 phosphorylation induced by VSV infection at MOI = 5 for 6 hr was detected by western blotting with anti-p-IRF3, anti-IRF3, and anti-β-actin antibodies (I). VSV-induced IFN-β mRNA expression was determined by qRT-PCR (J).

(K) HEK293 cells cultured in medium supplemented with 0 or 10 ng/ml EGF were transfected with IFN-β reporter (p125 luc) and MAVS expressing plasmid together with *Renilla* luciferase vector. 24 hr after transfection, luciferase activity was determined.

(L) HEK293 cells cultured in medium supplemented with 0 or 10 ng/ml EGF were transfected with vector expressing WT DDX60 or DDX60-YF mutant or empty vector, plus IFN-β reporter and *Renilla* luciferase plasmids. 24 hr after transfection, cells were stimulated with short polyI:C for 8 hr by transfection, and luciferase activity was determined.

(M) WT and *DDX60*-KO immortalized MEFs were cultured in medium supplemented with or without 10 ng/ml EGF. Short polyI:C-induced luciferase activity was determined as in (G).

(N and O) HeLa cells cultured in serum-free medium were infected with flu for 16 hr, then fixed and labeled with anti-DDX60 and anti-p-Y antibody. Colocalization of p-Y and DDX60 (p-Y-DDX60) was detected by PLA (N). The number of colocalization signals (PLA signals) per cell was counted (O). Data are presented as mean ± SD (n > 10).

(P and Q) HeLa cell were mock-infected or infected with influenza A virus at MOI = 10 and fixed at indicated time points. Co-localization of DDX60 and EGF receptor (EGFR) was detected by PLA using anti-DDX60 and anti-EGFR antibodies (P). The ratio of the PLA-positive cells is shown (Q).

(R) WT and *DDX60* KO MEFs were cultured in serum-free medium supplemented with 0 or 10 ng/ml EGF for 24 hr and then infected with VSV at MOI = 1. Total RNA was extracted at the indicated time points, and IFN-β and IFN-λ2/3 mRNA expression was determined by qRT-PCR.

The scale bar represents 10 μm. See also Figure S6.

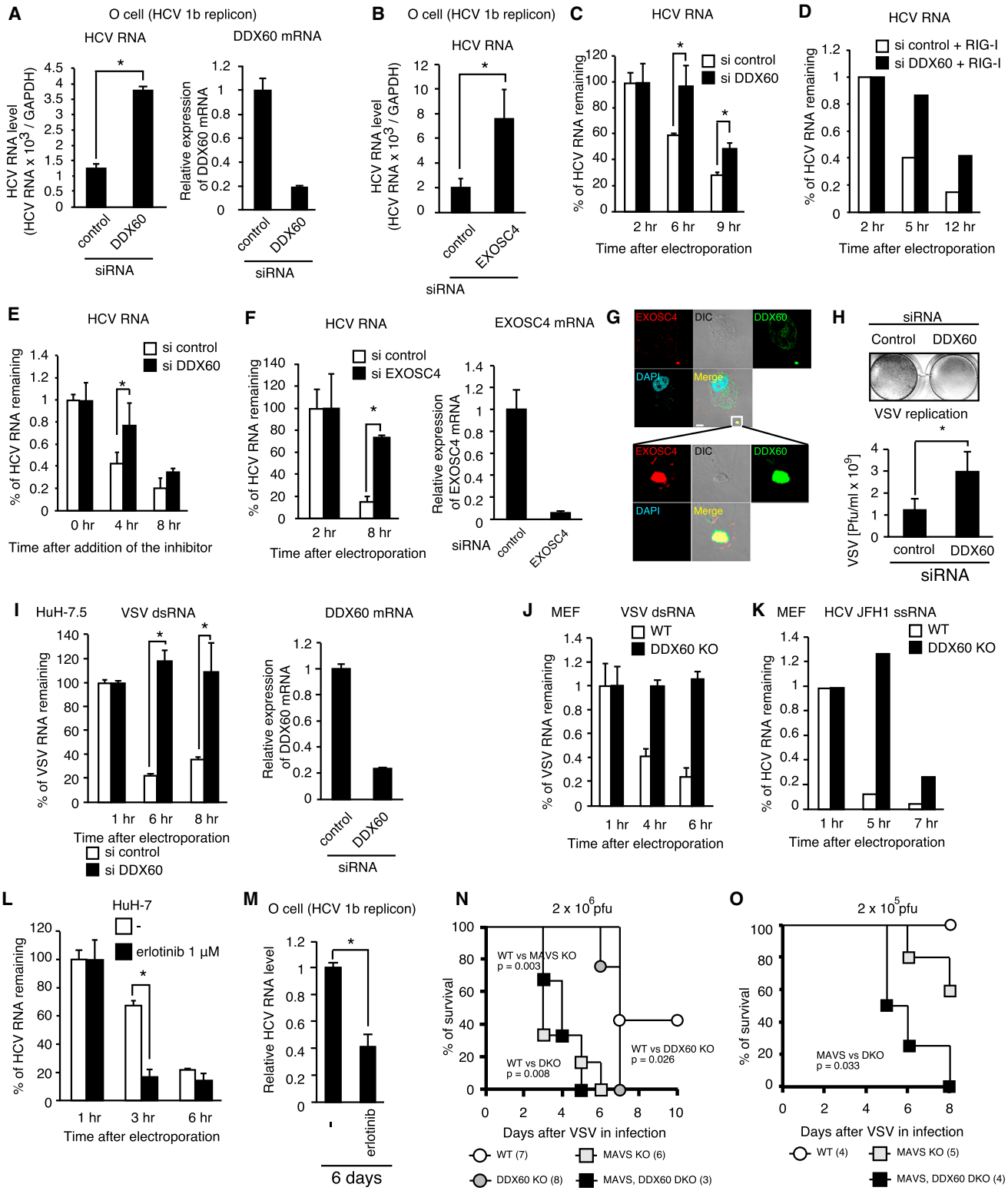

Figure 7. DDX60 Promotes Viral RNA Degradation

(A and B) siRNA for negative control, *DDX60* (A), or *EXOSC4* (B) was transfected into O cells with HCV replicons for 48 hr (A) or 72 hr (B), then HCV RNA levels were determined by qRT-PCR. The results are expressed as mean ± SD (n = 3).

(legend continued on next page)

MEFs, peritoneal macrophages, and splenic CD11c$^+$ cells required DDX60 for efficient type I IFN production, whereas BM-DCs did not. These data indicate a cell-type-specific role of DDX60. Because other DDX helicases are also involved in RIG-I-mediated type I IFN production and highly expressed in BM-DCs, those helicases might function as sentinels for RIG-I and compensate for the defect of DDX60. Interestingly, Liu and colleagues reported a cell-type-specific role of DHX29 (Sugimoto et al., 2014). These data indicate that there are several cell-type-specific sentinel helicases for RIG-I activation.

Rice and colleagues showed that DDX60 antiviral activity is specific for HCV and does not require RIG-I (Schoggins et al., 2011). They used STAT-1-deficient cells, in which type I IFN induced by RIG-I signaling cannot activate the antiviral response (Schoggins et al., 2011). Here, we demonstrated that DDX60 was involved not only in RIG-I-mediated type I IFN signaling but also in the RIG-I-independent HCV RNA degradation pathway. This finding is consistent with the results of the previous study by Rice and colleagues (Schoggins et al., 2011). DDX60 was involved in VSV RNA degradation, and *DDX60* and *MAVS* double-KO mice were more susceptible to VSV infection than *MAVS* single-KO mice. These data indicate that DDX60-mediated viral RNA degradation plays a crucial role in antiviral response in vivo.

Here, we revealed a regulatory mechanism of EGF-receptor-mediated suppression of DDX60 antiviral activity. EGF signaling induced DDX60 Tyr phosphorylation, resulting in malfunction of its ATP binding activity required for antiviral activity. We also found that EGF treatment induced DDX60 aggregation in the cytoplasm. The aggregates might sequestrate or inhibit virus-induced DDX60 and/or RIG-I at a later phase. Further study is required to clarify the physiological significance of the cytoplasmic DDX60 aggregates induced by EGF signaling.

A recent study revealed that EGF signaling inhibited IRF1-mediated type III IFN production (Ueki et al., 2013). Considering that RIG-I activates IRF1 to induce type III IFN (Odendall et al., 2014), EGF-signaling-mediated suppression of IRF1 might be caused by DDX60 phosphorylation. On the other hand, it has been reported that EGF signaling reduced STAT1 dimerization (Lupberger et al., 2013). These observations imply that EGF receptor activation inhibits several steps of antiviral innate immune responses. A previous study demonstrates that inhibitors for EGF receptor suppress HCV infection in a human liver chimeric mouse model in vivo (Lupberger et al., 2011). Therefore, virus-mediated EGF receptor activation is important for virus to escape the host innate immune response in vivo. Because various types of viruses activate EGF receptor to facilitate their replication (Ueki et al., 2013), our findings provide an insight into the mechanism underlying the promotion of viral infection and replication by virus-mediated EGF receptor activation.

Unlike what was observed for DDX60, EGF-receptor-mediated Tyr phosphorylation is essential for the activation of TLR3, which recognizes viral RNA (Yamashita et al., 2012). Thus, a high EGF concentration is expected to promote the TLR3-mediated, but not the DDX60-mediated, innate immune response. TLR3 promotes cross-priming and activates cytotoxic T lymphocytes (Schulz et al., 2005). Conversely, the RIG-I pathway is required for initial antiviral responses (Koyama et al., 2007). Serum EGF and EGF receptor expression levels on the cell surface are reduced during aging (Shurin et al., 2007). Thus, EGF-mediated control of the innate immune responses may be a cause of age-dependent functional changes in innate immunity.

EXPERIMENTAL PROCEDURES

Cells, Viruses, and Reagents

Cell culture media for HEK293, HeLa, O, HuH-7, and HuH-7.5 cells were described previously (Oshiumi et al., 2009, 2013). Preparation of mouse BM-DCs and peritoneal macrophages was described previously (Oshiumi et al., 2010a). WT and *DDX60*$^{-/-}$ MEFs were prepared from day 12.5 to day 14.5 embryos. MEFs were immortalized using large T antigen of SV40. Preparation of VSV Indiana strain, SeV (HVJ strain), and HSV-1 was described previously (Miyashita et al., 2011). Influenza A virus (PR8) was provided by Y. Sakoda (Hokkaido University). We used salmon sperm dsDNA (Invitrogen), erlotinib (Funakoshi), mouse recombinant EGF, (Wako), anti-DDX60 polyclonal antibody (SIGMA), anti-HA polyclonal antibody (SIGMA), anti-β-actin monoclonal antibody (AC-15) (SIGMA), anti-RIG-I monoclonal antibody (Alme-1) (Axxora Platform), anti-G3BP antibody (Abcam), anti-NAK (TBK1) antibody (EP611Y) (Abcam), anti-p-TBK1 rabbit monoclonal antibody (CST), anti-p-IRF3 (S396) rabbit monoclonal antibody (CST), and anti-IRF3 antibody (Invitrogen and Zymed). Preparation of viral RNA is described in Supplemental Experimental Procedures.

Electroporation

1 μg viral RNA (HCV JFH-1 GND ssRNA or VSV dsRNA) and 1 × 10^6 cells were suspended in 400 μl of OPTI-MEM I in a 4-mm cuvette and pulsed once at

(C and D) HuH-7.5 (C) or HuH-7 (D) cells were transfected with siRNA for negative control, *DDX60*, and/or *RIG-I* for 48 hr, and then in vitro synthesized HCV JFH-1 GND RNA was electroporated into the cells. HCV RNA levels were determined by RT-qPCR.

(E) siRNA for negative control or *DDX60* were transfected into HuH-7.5 cells prior to HCV JFH1 infection. 3 days after infection, MK-0608 (final concentration, 35 μM) was added to cells, after which HCV RNA levels at the indicated time points were determined by qRT-PCR.

(F) HuH-7.5 cells were transfected with negative control or *EXOSC4* siRNA (C) for 48 hr, then in vitro synthesized HCV JFH-1 GND RNA was electroporated into the cells. HCV and *EXOSC4* RNA levels were determined by qRT-PCR.

(G) FLAG-tagged EXOSC4 was transiently expressed in O cells. Cells were fixed and stained with anti-DDX60 and anti-FLAG antibodies.

(H) HuH-7.5 cells were pre-treated with 200 IU of IFN-α for 24 hr and subsequently infected with VSV at MOI = 0.01 for 24 hr. Cells were fixed and stained with crystal violet (upper panel). VSV titer in culture medium of the IFN-α treated cells was determined by plaque assay (lower panel).

(I–K) VSV dsRNA (I, J) or HCV JFH1-GND ssRNA (K) were electroporated into control or *DDX60*-knockdown HuH-7.5 cells (I) or WT and *DDX60*-KO MEFs (J and K). Viral RNA levels at the indicated time points were determined by qRT-PCR.

(L) HuH-7 cells cultured with or without 1 μM erlotinib for 48 hr were electroporated with HCV JFH-1-GND RNA. HCV RNA levels were determined by qRT-PCR.

(M) O cells with HCV replicons were treated with 1 μM of erlotinib for 6 days. The cell culture medium containing erlotinib was replaced every 2 days. HCV RNA levels were determined by qRT-PCR.

(N and O) Wild-type (WT), *DDX60* single-KO, *MAVS* single-KO, and *DDX60*/*MAVS* double-KO mice were intranasally infected with 2 × 10^6 PFU of VSV (N) or 2 × 10^5 PFU of VSV (O), and mice mortality was observed.

250 V, 950 μF for HuH-7 and HuH-7.5 or at 400 V, 250 μF for MEFs in a Gene Pulser II System (Bio-Rad).

Pull-Down Assay

An ATP affinity test kit was purchased from JENA BIOSCIENCE. 6AH-ATP-agarose, 8AH-ATP-agarose, AP-ATP-agarose, and EDA-ATP-agarose were mixed. An ATP affinity test was conducted according to the manufacturer's instructions. A pull-down assay using biotin-conjugated dsRNA was described previously (Oshiumi et al., 2013).

Treatment with EGF

To examine the effect of EGF on short polyI:C-induced IFN-β promoter activation, EGF was added to medium for HEK293 and HuH-7 cells 24 hr before transfection. Cells were transfected with p125luc reporter, *Renilla* luciferase vector (internal control), and short polyI:C for 24 hr. To investigate the effect of DDX60-YF mutation, EGF was added to media of HEK293 cells 24 hr before transfection. Cells were transfected with p125luc reporter, *Renilla* luciferase vector, and WT DDX60 or DDX60-YF encoding vector for 24 hr and transfected with short polyI:C for 8 hr. To investigate the effect of EGF on IFN-β, IP10, and TNF-α mRNA expression after VSV or Flu infection, HeLa cells were cultured in serum-free media with or without EGF for 24 hr, and infected with VSV.

SUPPLEMENTAL INFORMATION

Supplemental Information includes Supplemental Experimental Procedures and six figures and can be found with this article online at http://dx.doi.org/10.1016/j.celrep.2015.04.047.

AUTHOR CONTRIBUTIONS

Y.M. and M. Okabe generated *DDX60*-deficient mice. H.O., M. Miyashita, and M. Okamoto performed all other experiments. H.O. designed the experiments and wrote the manuscript. M. Matsumoto and T.S. supervised the research.

ACKNOWLEDGMENTS

We thank Dr. A. Chan (Genentech), Dr. M. Kohara (Tokyo Metropolitan Institute of Medical and Science), and Dr. K. Shimotohno (National Center for Global Health and Medicine) for critical comments, and we thank and all colleagues in our laboratory. A plasmid encoding HCV JFH-1-GND (pSGR-JFH-1-GND) and O cells were kindly gifted from Dr. T. Wakita (National Institute of Infectious Disease) and Dr. N. Kato (Okayama University), respectively. This work was supported in part by Kato Memorial Bioscience Foundation and Grants-in-Aid from Ministry of Education, Science, and Culture and Ministry of Health, Labor, and Welfare of Japan and by the GI-CoRE project.

Received: June 27, 2014
Revised: March 12, 2015
Accepted: April 22, 2015
Published: May 14, 2015

REFERENCES

Chan, Y.K., and Gack, M.U. (2015). RIG-I-like receptor regulation in virus infection and immunity. Curr. Opin. Virol. *12C*, 7–14.

Chen, G., Guo, X., Lv, F., Xu, Y., and Gao, G. (2008). p72 DEAD box RNA helicase is required for optimal function of the zinc-finger antiviral protein. Proc. Natl. Acad. Sci. USA *105*, 4352–4357.

Desmet, C.J., and Ishii, K.J. (2012). Nucleic acid sensing at the interface between innate and adaptive immunity in vaccination. Nat. Rev. Immunol. *12*, 479–491.

Diao, J., Pantua, H., Ngu, H., Komuves, L., Diehl, L., Schaefer, G., and Kapadia, S.B. (2012). Hepatitis C virus induces epidermal growth factor receptor activation via CD81 binding for viral internalization and entry. J. Virol. *86*, 10935–10949.

Gao, D., Wu, J., Wu, Y.T., Du, F., Aroh, C., Yan, N., Sun, L., and Chen, Z.J. (2013). Cyclic GMP-AMP synthase is an innate immune sensor of HIV and other retroviruses. Science *341*, 903–906.

Guo, X., Ma, J., Sun, J., and Gao, G. (2007). The zinc-finger antiviral protein recruits the RNA processing exosome to degrade the target mRNA. Proc. Natl. Acad. Sci. USA *104*, 151–156.

Houseley, J., LaCava, J., and Tollervey, D. (2006). RNA-quality control by the exosome. Nat. Rev. Mol. Cell Biol. *7*, 529–539.

Jarvius, M., Paulsson, J., Weibrecht, I., Leuchowius, K.J., Andersson, A.C., Wählby, C., Gullberg, M., Botling, J., Sjöblom, T., Markova, B., et al. (2007). In situ detection of phosphorylated platelet-derived growth factor receptor beta using a generalized proximity ligation method. Mol. Cell. Proteomics *6*, 1500–1509.

Kingston, R.E., and Narlikar, G.J. (1999). ATP-dependent remodeling and acetylation as regulators of chromatin fluidity. Genes Dev. *13*, 2339–2352.

Kondo, T., Kobayashi, J., Saitoh, T., Maruyama, K., Ishii, K.J., Barber, G.N., Komatsu, K., Akira, S., and Kawai, T. (2013). DNA damage sensor MRE11 recognizes cytosolic double-stranded DNA and induces type I interferon by regulating STING trafficking. Proc. Natl. Acad. Sci. USA *110*, 2969–2974.

Koyama, S., Ishii, K.J., Kumar, H., Tanimoto, T., Coban, C., Uematsu, S., Kawai, T., and Akira, S. (2007). Differential role of TLR- and RLR-signaling in the immune responses to influenza A virus infection and vaccination. J. Immunol. *179*, 4711–4720.

Li, X.D., Wu, J., Gao, D., Wang, H., Sun, L., and Chen, Z.J. (2013a). Pivotal roles of cGAS-cGAMP signaling in antiviral defense and immune adjuvant effects. Science *341*, 1390–1394.

Li, Y., Masaki, T., Yamane, D., McGivern, D.R., and Lemon, S.M. (2013b). Competing and noncompeting activities of miR-122 and the 5′ exonuclease Xrn1 in regulation of hepatitis C virus replication. Proc. Natl. Acad. Sci. USA *110*, 1881–1886.

Loo, Y.M., and Gale, M., Jr. (2011). Immune signaling by RIG-I-like receptors. Immunity *34*, 680–692.

Lupberger, J., Zeisel, M.B., Xiao, F., Thumann, C., Fofana, I., Zona, L., Davis, C., Mee, C.J., Turek, M., Gorke, S., et al. (2011). EGFR and EphA2 are host factors for hepatitis C virus entry and possible targets for antiviral therapy. Nat. Med. *17*, 589–595.

Lupberger, J., Duong, F.H., Fofana, I., Zona, L., Xiao, F., Thumann, C., Durand, S.C., Pessaux, P., Zeisel, M.B., Heim, M.H., and Baumert, T.F. (2013). Epidermal growth factor receptor signaling impairs the antiviral activity of interferon-alpha. Hepatology *58*, 1225–1235.

Miyashita, M., Oshiumi, H., Matsumoto, M., and Seya, T. (2011). DDX60, a DEXD/H box helicase, is a novel antiviral factor promoting RIG-I-like receptor-mediated signaling. Mol. Cell. Biol. *31*, 3802–3819.

Odendall, C., Dixit, E., Stavru, F., Bierne, H., Franz, K.M., Durbin, A.F., Boulant, S., Gehrke, L., Cossart, P., and Kagan, J.C. (2014). Diverse intracellular pathogens activate type III interferon expression from peroxisomes. Nat. Immunol. *15*, 717–726.

Okamoto, M., Oshiumi, H., Azuma, M., Kato, N., Matsumoto, M., and Seya, T. (2014). IPS-1 is essential for type III IFN production by hepatocytes and dendritic cells in response to hepatitis C virus infection. J. Immunol. *192*, 2770–2777.

Onomoto, K., Jogi, M., Yoo, J.S., Narita, R., Morimoto, S., Takemura, A., Sambhara, S., Kawaguchi, A., Osari, S., Nagata, K., et al. (2012). Critical role of an antiviral stress granule containing RIG-I and PKR in viral detection and innate immunity. PLoS ONE *7*, e43031.

Oshiumi, H., Matsumoto, M., Hatakeyama, S., and Seya, T. (2009). Riplet/RNF135, a RING finger protein, ubiquitinates RIG-I to promote interferon-beta induction during the early phase of viral infection. J. Biol. Chem. *284*, 807–817.

Oshiumi, H., Miyashita, M., Inoue, N., Okabe, M., Matsumoto, M., and Seya, T. (2010a). The ubiquitin ligase Riplet is essential for RIG-I-dependent innate immune responses to RNA virus infection. Cell Host Microbe *8*, 496–509.

Oshiumi, H., Sakai, K., Matsumoto, M., and Seya, T. (2010b). DEAD/H BOX 3 (DDX3) helicase binds the RIG-I adaptor IPS-1 to up-regulate IFN-beta inducing potential. Eur. J. Immunol. *40*, 940–948.

Oshiumi, H., Miyashita, M., Matsumoto, M., and Seya, T. (2013). A distinct role of Riplet-mediated K63-Linked polyubiquitination of the RIG-I repressor domain in human antiviral innate immune responses. PLoS Pathog. *9*, e1003533.

Saito, T., Hirai, R., Loo, Y.M., Owen, D., Johnson, C.L., Sinha, S.C., Akira, S., Fujita, T., and Gale, M., Jr. (2007). Regulation of innate antiviral defenses through a shared repressor domain in RIG-I and LGP2. Proc. Natl. Acad. Sci. USA *104*, 582–587.

Saito, T., Owen, D.M., Jiang, F., Marcotrigiano, J., and Gale, M., Jr. (2008). Innate immunity induced by composition-dependent RIG-I recognition of hepatitis C virus RNA. Nature *454*, 523–527.

Schmid, M., and Jensen, T.H. (2008). The exosome: a multipurpose RNA-decay machine. Trends Biochem. Sci. *33*, 501–510.

Schoggins, J.W., Wilson, S.J., Panis, M., Murphy, M.Y., Jones, C.T., Bieniasz, P., and Rice, C.M. (2011). A diverse range of gene products are effectors of the type I interferon antiviral response. Nature *472*, 481–485.

Schröder, M., Baran, M., and Bowie, A.G. (2008). Viral targeting of DEAD box protein 3 reveals its role in TBK1/IKKepsilon-mediated IRF activation. EMBO J. *27*, 2147–2157.

Schulz, O., Diebold, S.S., Chen, M., Näslund, T.I., Nolte, M.A., Alexopoulou, L., Azuma, Y.T., Flavell, R.A., Liljeström, P., and Reis e Sousa, C. (2005). Toll-like receptor 3 promotes cross-priming to virus-infected cells. Nature *433*, 887–892.

Sedano, C.D., and Sarnow, P. (2014). Hepatitis C virus subverts liver-specific miR-122 to protect the viral genome from exoribonuclease Xrn2. Cell Host Microbe *16*, 257–264.

Shurin, G.V., Yurkovetsky, Z.R., Chatta, G.S., Tourkova, I.L., Shurin, M.R., and Lokshin, A.E. (2007). Dynamic alteration of soluble serum biomarkers in healthy aging. Cytokine *39*, 123–129.

Solinger, J.A., Kiianitsa, K., and Heyer, W.D. (2002). Rad54, a Swi2/Snf2-like recombinational repair protein, disassembles Rad51:dsDNA filaments. Mol. Cell *10*, 1175–1188.

Soulat, D., Bürckstümmer, T., Westermayer, S., Goncalves, A., Bauch, A., Stefanovic, A., Hantschel, O., Bennett, K.L., Decker, T., and Superti-Furga, G. (2008). The DEAD-box helicase DDX3X is a critical component of the TANK-binding kinase 1-dependent innate immune response. EMBO J. *27*, 2135–2146.

Sugimoto, N., Mitoma, H., Kim, T., Hanabuchi, S., and Liu, Y.J. (2014). Helicase proteins DHX29 and RIG-I cosense cytosolic nucleic acids in the human airway system. Proc. Natl. Acad. Sci. USA *111*, 7747–7752.

Sun, L., Wu, J., Du, F., Chen, X., and Chen, Z.J. (2013). Cyclic GMP-AMP synthase is a cytosolic DNA sensor that activates the type I interferon pathway. Science *339*, 786–791.

Takahasi, K., Yoneyama, M., Nishihori, T., Hirai, R., Kumeta, H., Narita, R., Gale, M., Jr., Inagaki, F., and Fujita, T. (2008). Nonself RNA-sensing mechanism of RIG-I helicase and activation of antiviral immune responses. Mol. Cell *29*, 428–440.

Tong, J., Taylor, P., Jovceva, E., St-Germain, J.R., Jin, L.L., Nikolic, A., Gu, X., Li, Z.H., Trudel, S., and Moran, M.F. (2008). Tandem immunoprecipitation of phosphotyrosine-mass spectrometry (TIPY-MS) indicates C19ORF19 becomes tyrosine-phosphorylated and associated with activated epidermal growth factor receptor. J. Proteome Res. *7*, 1067–1077.

Ueki, I.F., Min-Oo, G., Kalinowski, A., Ballon-Landa, E., Lanier, L.L., Nadel, J.A., and Koff, J.L. (2013). Respiratory virus-induced EGFR activation suppresses IRF1-dependent interferon λ and antiviral defense in airway epithelium. J. Exp. Med. *210*, 1929–1936.

Yamashita, M., Chattopadhyay, S., Fensterl, V., Saikia, P., Wetzel, J.L., and Sen, G.C. (2012). Epidermal growth factor receptor is essential for Toll-like receptor 3 signaling. Sci. Signal. *5*, ra50.

Yanai, H., Ban, T., Wang, Z., Choi, M.K., Kawamura, T., Negishi, H., Nakasato, M., Lu, Y., Hangai, S., Koshiba, R., et al. (2009). HMGB proteins function as universal sentinels for nucleic-acid-mediated innate immune responses. Nature *462*, 99–103.

Yoo, J.S., Takahasi, K., Ng, C.S., Ouda, R., Onomoto, K., Yoneyama, M., Lai, J.C., Lattmann, S., Nagamine, Y., Matsui, T., et al. (2014). DHX36 enhances RIG-I signaling by facilitating PKR-mediated antiviral stress granule formation. PLoS Pathog. *10*, e1004012.